ROLE OF THE DEFORMATION OF MULTIPOLARITY SIX IN THE DYNAMIC DESCRIPTION OF SPONTANEOUS FISSION*

By K. Böning and A. Sobiczewski

Institute for Nuclear Research, Warsaw**

(Received August 31, 1982)

The role of the deformation of multipolarity six, ε_6, in the description of spontaneous-fission half-lives is studied. Doubly even heavy nuclei ($Z = 92$–102) are considered. It is found that inclusion of ε_6 may change the half-lives by up to about four orders. The structure of the microscopic inertia (mass) tensor, connected with ε_6, is also investigated. Finally, the equilibrium values of ε_6 are calculated. It appears that these quantities are of dynamic rather than static nature.

PACS numbers: 24.80.+y, 21.10.Ft

1. Introduction

This study belongs to a series of papers [1–3] in which the spontaneous-fission characteristics: barriers and half-lives are described without use of any adjustable parameters. It has been found [3] that such description allows us to reproduce the half-lives of even-even heavy nuclei, measured for 40 nuclides ($Z = 92$–104), within a factor of about 50, on the average, i.e. fairly well.

The penetration of the fission barrier is treated dynamically [4]. One of the main things, which are decisive for the results, is how rich is the deformation space admitted in the calculations. In our previous analysis [3], the deformations of multipolarity 2, 3, 4 and in some approximation also 5 were considered dynamically. The deformation of multipolarity 6 has been treated only statically.

The main scope of the present paper is to investigate the role of this deformation when treated dynamically. Additional scope is a study of the components of the mass tensor associated with the deformation of multipolarity 6, not investigated up to now, and also the equilibrium values of this deformation for even-even nuclei of actinides.

* Supported in part by the Polish–USA Maria Skłodowska-Curie Fund. Grant No. P-F7F037P.

** Address: Instytut Badań Jądrowych, Hoża 69, 00-681 Warszawa, Poland.

2. *Description of the calculations*

The calculations are performed in the way very similar to that of our previous paper [3]. Due to this, we present here only the main points, referring to that paper for details. We also stress here the differences between the two calculations.

The main problem in determining the fission half-life is the problem of penetration of the fission barrier by a nucleus. In the one-dimensional quasi-classical (WKB) approximation, the problem reduces to the question of finding the trajectory $L_{\min}$, given in the deformation space, along which the action integral

$$S(L) = 2\int_{s_1}^{s_2} \sqrt{\frac{2}{\hbar^2}[V(s)-E]B_s(s)}\,ds \tag{1}$$

is minimal. Here, $V(s)$ is the potential energy, $B_s(s)$ is the effective inertia (mass) along L and E is the energy of a fissioning nucleus. The parameter s specifies the position of a point on the trajectory L, with s_1 and s_2 corresponding to the classical turning points satisfying the condition: $V(s) = E$. The effective inertia $B_s(s)$ associated with the fission motion along the trajectory L is

$$B_s(s) \equiv B_{ss}(s) = \sum_{ij} B_{\alpha_i\alpha_j}(s)\frac{d\alpha_i}{ds}\frac{d\alpha_j}{ds}, \tag{2}$$

where $B_{\alpha_i\alpha_j}$ are components of the inertia tensor and α_i, α_j $(i, j = 1, 2, \ldots, M)$ are the deformation parameters specifying the M-dimensional deformation space admitted in the description of the fission motion.

Similarly as in the previous paper [3], we admit a four-dimensional deformation space, described by the four Nilsson deformation parameters [5]: ε, ε_4, ε_{35} and ε_6, corresponding to the deformations of multipolarity 2 (quadrupole), 4 (hexadecapole), 3 combined with 5, and 6, respectively.

Minimization of the action integral (1) is not, however, performed in the full four-dimensional space. It is approximated by a sequence of three two-dimensional minimizations performed in three two-dimensional spaces. The spaces are the planes crossing each other along the straight line $\bar{L}$

$$\bar{\varepsilon}_4(\varepsilon) = 0.2\varepsilon - 0.06, \quad \bar{\varepsilon}_{35} = 0, \quad \bar{\varepsilon}_6 = 0, \tag{3}$$

being an average minimal trajectory for all investigated nuclei [3]. The three planes are: $(\varepsilon, \varepsilon_4)$, $(\varepsilon, \varepsilon_{35})$ and $(\varepsilon, \varepsilon_6)$, or in the notation explicitly taking into account [3] that they contain the line $\bar{L}$: $(\varepsilon, \varepsilon_4)$, $(\varepsilon_{24}, \varepsilon_{35})$ and $(\varepsilon_{24}, \varepsilon_6)$.

An analysis performed in each plane gives a contribution to the total spontaneous-fission half-life (as well as to the barrier)

$$T_{sf} = \bar{T} \cdot \Delta T_{35} \cdot \Delta T_4 \cdot \Delta T_6, \tag{4}$$

where $\bar{T}$ is the half-life calculated along the average trajectory $\bar{L}$ and the corrections ΔT_{35}, ΔT_4, ΔT_6 are obtained in the analyses in the planes $(\varepsilon_{24}, \varepsilon_{35})$, $(\varepsilon, \varepsilon_4)$, $(\varepsilon_{24}, \varepsilon_6)$, respectively.

To make the corrections as small as possible, we use the potential energy which gives the fission barrier as realistic as possible in each plane. To be more specific, for a given plane, the energy is minimized with respect to all deformations which do not explicitly appear in the plane. The minimization is performed in an approximate, one-dimensional way. With all deformations, except one ε_i, fixed at a given point P at the average path $\bar{L}$: $\varepsilon_j(\varepsilon) = \bar{\varepsilon}_j$ $(j \neq i)$, the energy is minimized with respect to ε_i. This allows us to get the difference

$$\Delta V_i(\varepsilon) = V(\varepsilon, \bar{\varepsilon}_4, \bar{\varepsilon}_{35}, \ldots, \varepsilon_i^{\min}, \ldots) - V(\varepsilon, \bar{\varepsilon}_4, \bar{\varepsilon}_{35}, \ldots, \bar{\varepsilon}_i, \ldots), \tag{5}$$

where $\varepsilon_i^{\min}$ denotes the value of ε_i at which the energy V is minimal. The quantity ΔV_i is a function of only a point P on $\bar{L}$ and thus only of the deformation ε, which describes the position of P on $\bar{L}$. It corrects the potential energy for effect of the deformation ε_i, which does not explicitly appear in a given plane.

For example, in the $(\varepsilon, \varepsilon_{35})$-plane, the potential energy is

$$V = V(\varepsilon, \bar{\varepsilon}_4, \varepsilon_{35}, 0) + \Delta V_4(\varepsilon) + \Delta V_6(\varepsilon), \tag{6}$$

where

$$\Delta V_4(\varepsilon) = V(\varepsilon, \varepsilon_4^{\min}, 0, 0) - V(\varepsilon, \bar{\varepsilon}_4, 0, 0),$$

$$\Delta V_6(\varepsilon) = V(\varepsilon, \bar{\varepsilon}_4, 0, \varepsilon_6^{\min}) - V(\varepsilon, \bar{\varepsilon}_4, 0, 0).$$

(Here, we have already taken into account the fact that our average path is of the form of Eq. (3), i.e. that $\bar{\varepsilon}_{35} = \bar{\varepsilon}_6 = 0$). Thus, for each point $(\varepsilon, \varepsilon_{35})$ of the $(\varepsilon, \varepsilon_{35})$-plane, the energy is calculated with ε and ε_{35} taken exactly at this point and with the remaining deformations ε_4, ε_6 taken from the average path $\bar{L}$: $\varepsilon_4 = \bar{\varepsilon}_4(\varepsilon)$, $\varepsilon_6 = \bar{\varepsilon}_6(\varepsilon)$. This energy is then improved by the corrections $\Delta V_4(\varepsilon)$ and $\Delta V_6(\varepsilon)$, corresponding to these remaining deformations and calculated according to Eq. (5).

In the present paper, we are only interested in the analysis in the $(\varepsilon_{24}, \varepsilon_6)$-plane. In the other planes, the analyses have been performed in our previous paper [3]. The potential energy and the components: $B_{\varepsilon_{24}\varepsilon_{24}}$, $B_{\varepsilon_{24}\varepsilon_6}$, $B_{\varepsilon_6\varepsilon_6}$ of the mass tensor are calculated in the grid points

$$\varepsilon = 0(0.05)1.0, \quad \varepsilon_6 = -0.04(0.01)0.04, \tag{7}$$

i.e. in the $21 \times 9 = 189$ points. Thus, the points are here taken more densely, in ε_6, than in Ref. [3].

The macroscopic part of the potential energy is taken from the droplet model with the parameters of Ref. [6], i.e. the same as used in paper [2]. The effect of using the parameters of Ref. [7] (i.e. the same as used in paper [3]), instead of those of Ref. [6], on the quantities investigated here is small.

The microscopic calculations are based on the Nilsson potential with the "$A = 242$" parameters [5] and on the pairing interaction with the strength independent of deformation [5].

Minimization of the action integral, Eq. (1), is performed by the dynamic-programming method [3].

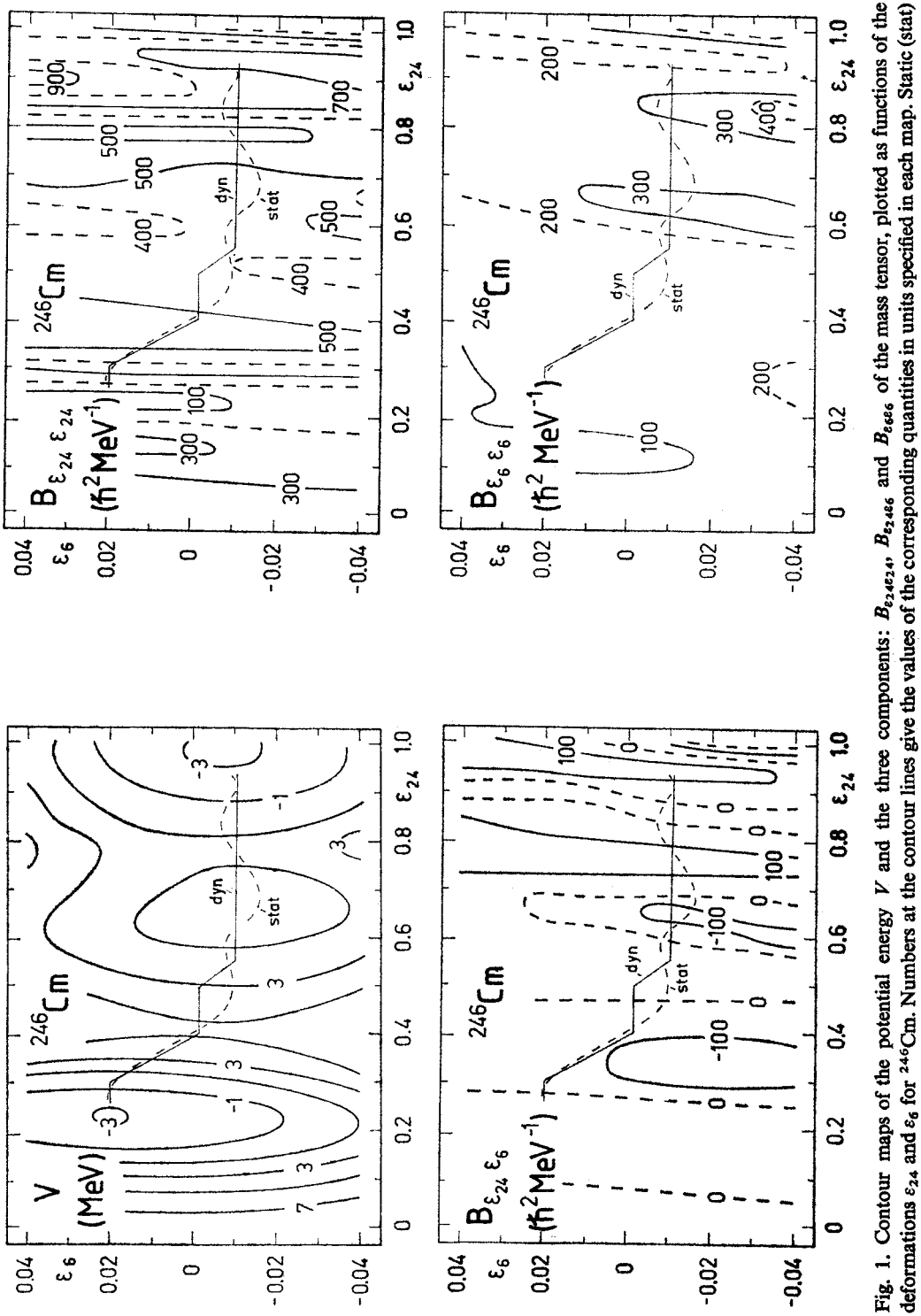

Fig. 1. Contour maps of the potential energy V and the three components: $B_{\varepsilon_{24}\varepsilon_{24}}$, $B_{\varepsilon_{24}\varepsilon_6}$ and $B_{\varepsilon_6\varepsilon_6}$ of the mass tensor, plotted as functions of the deformations ε_{24} and ε_6 for ^{246}Cm. Numbers at the contour lines give the values of the corresponding quantities in units specified in each map. Static (stat) and dynamic (dyn) trajectories are indicated

3. *Results and discussion*

For a detailed illustration of the results, we choose the nucleus ^{246}Cm, the same as in the previous paper [3].

3.1. Potential energy and mass tensor

Fig. 1. presents the potential energy V and the three components: $B_{\varepsilon_{24}\varepsilon_{24}}$, $B_{\varepsilon_{24}\varepsilon_6}$, $B_{\varepsilon_6\varepsilon_6}$ of the mass tensor as functions of the deformations ε_{24} and ε_6. The potential energy, plotted here as an explicit function of only the deformations ε_{24} and ε_6 is minimized with respect to the other considered deformations, ε_4 and ε_{35}, as described in the previous section. All four quantities show rather large fluctuations (as functions of the deformations) which are the result of the shell structure of the nucleus. Concerning the mass tensor, the largest values are obtained for the component $B_{\varepsilon_{24}\varepsilon_{24}}$. The non-diagonal component $B_{\varepsilon_{24}\varepsilon_6}$ is rather small. It fluctuates around zero with an amplitude of about 100 $\hbar^2$MeV^{-1}. Both static and dynamic fission trajectories are shown in the figure.

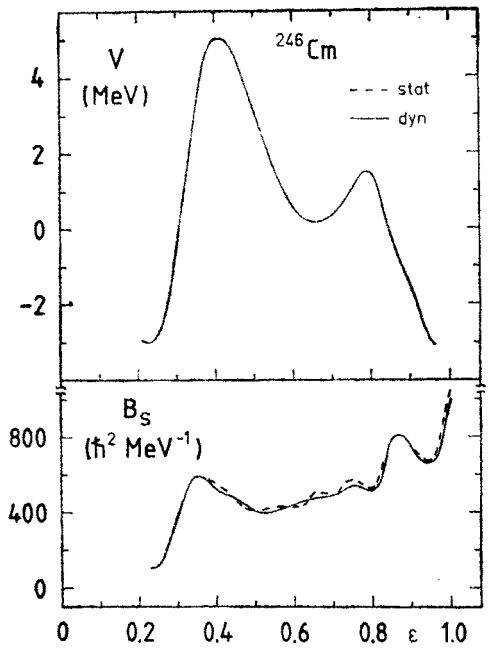

Fig. 2. Potential-energy barrier V and the effective mass parameter B_s plotted along static and dynamic trajectories in the $(\varepsilon_{24}, \varepsilon_6)$-plane for ^{246}Cm

Fig. 2 shows the potential-energy barrier V and the effective mass parameter B_s drawn along both the static and dynamic trajectories. The parameter B_s is, on the average, smaller and more smooth along the dynamic trajectory than along the static one. However, the difference between the two is much less than that obtained in the $(\varepsilon, \varepsilon_4)$-plane [3], both for V and B. In particular, the barriers along the dynamic and static trajectories differ less

than by 0.1 MeV and are indistinguishable in the figure. The smaller effects of dynamics in the $(\varepsilon_{24}, \varepsilon_6)$-plane than those in the $(\varepsilon, \varepsilon_4)$-plane are probably due to the smaller values of the mass parameters corresponding to the $(\varepsilon_{24}, \varepsilon_6)$-plane than those corresponding to the $(\varepsilon, \varepsilon_4)$-plane. To be more specific, the parameters $B_{\varepsilon_{24}\varepsilon_{24}}$, $B_{\varepsilon_{24}\varepsilon_6}$ and $B_{\varepsilon_6\varepsilon_6}$ are about 2–3 times smaller than the parameters $B_{\varepsilon\varepsilon}$, $B_{\varepsilon\varepsilon_4}$ and $B_{\varepsilon_4\varepsilon_4}$, respectively, as can be learned comparing the results of the present paper with those of the previous one [3].

3.2. Barriers and half-lives

Static effect of the deformation ε_6 on the potential-energy barrier is illustrated in Fig. 3 taken from Ref. [3]. One can see that this effect amounts to up to about 1 MeV. As stated in the previous subsection, the dynamics in the $(\varepsilon_{24}, \varepsilon_6)$-plane corrects the static barrier only very little (by less than 0.1 MeV for ^{246}Cm).

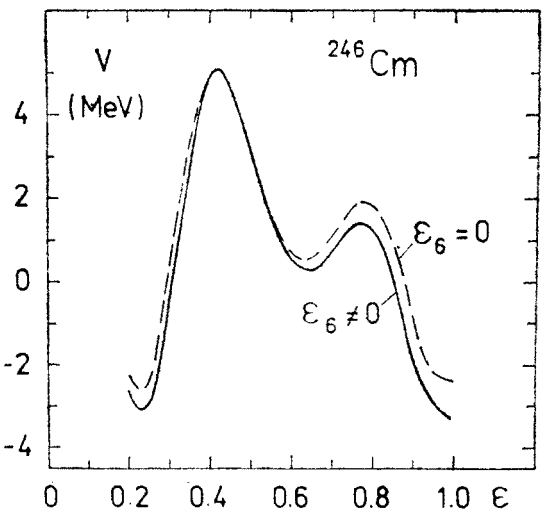

Fig. 3. Potential-energy barrier V along the $\varepsilon_6 = 0$ trajectory and along the static trajectory ($\varepsilon_6 \neq 0$) in the $(\varepsilon_{24}, \varepsilon_6)$-plane

Table I gives the dynamic corrections $\Delta T_6^{\mathrm{dyn}}$ to the half-lives T_{sf}, coming from the ε_6 degree of freedom. They are calculated for $6 \times 12 = 72$ isotopes of the $Z = 92$–102 elements. The correction is defined as the ratio of the half-life calculated along the dynamic trajectory in the $(\varepsilon_{24}, \varepsilon_6)$-plane to the half-life calculated along $\varepsilon_6 = 0$ line, i.e.

$$\Delta T_6^{\mathrm{dyn}} = \frac{T_6^{\mathrm{dyn}}[V(\varepsilon_{24}, \varepsilon_6), B(\varepsilon_{24}, \varepsilon_6)]}{T_6[V(\varepsilon_{24}, 0), B(\varepsilon_{24}, 0)]} .$$

For the nuclei with $Z = 96$–102, the corrections ΔT_6^V calculated in our previous paper [3], where the effect of ε_6 was accounted for only via the potential energy V, i.e.

$$\Delta T_6^V = \frac{T_6^{\mathrm{stat}}[V(\varepsilon_{24}, \varepsilon_6), B(\varepsilon_{24}, 0)]}{T_6[V(\varepsilon_{24}, 0), B(\varepsilon_{24}, 0)]}$$

TABLE I

Corrections ΔT_6^{dyn} and ΔT_6^V (second number for each nucleus with $Z = 96$–102) to half-lives T_{sf}, calculated as functions of the proton Z and neutron N numbers

Z \ N	138	140	142	144	146	148	150	152	154	156	158	160
92	−0.6	−0.5	−0.4	−0.2	0.0	0.6	0.9	1.2	1.2	1.0	0.9	0.8
94	−0.6	−0.6	−0.4	−0.1	0.3	1.1	1.4	2.0	1.4	1.2	1.1	1.1
96	−0.9	−0.7	−0.3	0.3	1.0	2.2	1.8	2.2	2.0	1.6	1.5	1.1
	−2.2	−2.6	−2.0	−1.6	−0.8	0.6	0.9	0.9	0.9	0.8	0.6	−0.2
98	−0.5	−0.4	0.3	0.7	1.6	2.3	2.4	2.6	2.5	2.2	2.1	2.2
	−1.3	−1.2	−0.8	−0.9	0.5	1.2	1.4	1.7	1.5	1.4	1.2	1.3
100	−0.4	−0.3	0.0	1.8	2.2	3.2	3.4	3.8	3.8	3.0	3.6	2.2
	−0.5	−0.4	−1.2	−0.2	1.2	1.8	0.9	2.5	2.4	2.0	2.0	1.0
102	−0.5	−0.4	−0.1	0.6	1.4	3.5	3.7	4.1	4.2	2.3	1.3	1.1
	−0.5	−0.5	−0.4	0.1	0.9	3.0	2.4	3.0	3.0	1.9	1.2	0.9

are also given. One can see that the more accurate dynamic corrections ΔT_6^{dyn} lead to longer lifetimes T_{sf}. The difference between the two amounts to up to 1.5 orders. The values of the dynamic correction ΔT_6^{dyn}, themselves, are from about one order of magnitude for lightest considered nuclei ($Z = 92$) up to about four orders for the heaviest ($Z = 102$).

Fig. 4 shows half-lives T_{sf} calculated: without any correction ΔT_6, with dynamic correction ΔT_6^{dyn} and with ΔT_6^V, for 12 isotopes of Cm. The experimental values are also

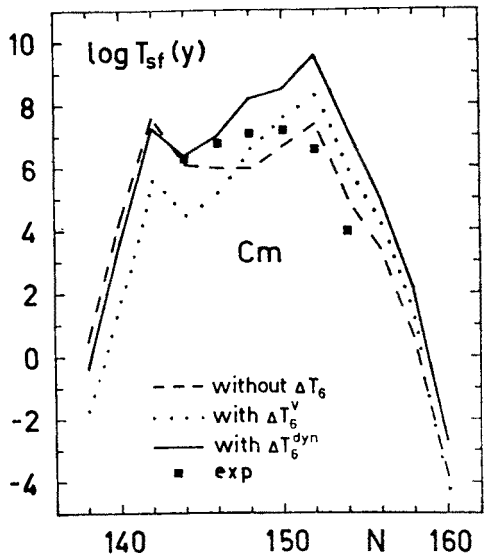

Fig. 4. Logarithms of the half-lives T_{sf} calculated: without any correction ΔT_6, with ΔT_6^V and with ΔT_6^{dyn}, for 12 isotopes of Cm. The experimental values are also shown

shown. One can see that T_{sf} calculated with ΔT_6^{dyn} are higher than the experimental values. The discrepancy is largest for the heaviest isotopes and is higher in the case of ΔT_6^{dyn} than of ΔT_6^{V}. This statement remains also true for the heavier elements: $Z = 98$–102.

To complete the discussion of various effects in T_{sf}, we have studied the effects of dynamics in the $(\varepsilon_{24}, \varepsilon_6)$-plane. We have namely studied the ratio of the dynamic value ΔT_6^{dyn} to the static one ΔT_6^{stat} defined as

$$\Delta T_6^{stat} = \frac{T_6^{stat}[V(\varepsilon_{24}, \varepsilon_6), B(\varepsilon_{24}, \varepsilon_6)]}{T_6[V(\varepsilon_{24}, 0), B(\varepsilon_{24}, 0)]} .$$

It is found that $\Delta T_6^{dyn}(T_6^{dyn})$ is smaller than $\Delta T_6^{stat}(T_6^{stat})$ by no more than 0.4 orders, for all investigated nuclei. Thus, the dynamical treatment of the lifetimes T_{sf} in the $(\varepsilon_{24}, \varepsilon_6)$-plane decreases them rather weakly. This is explicitly illustrated in Table II, for isotopes of Cm.

TABLE II

Effect of dynamics in the $(\varepsilon_{24}, \varepsilon_6)$-plane on T_{sf}, for Cm isotopes

N	138	140	142	144	146	148	150	152	154	156	158	160
$\log(\Delta T_6^{dyn}/\Delta T_6^{stat})$	−0.2	−0.1	0.0	−0.1	−0.2	−0.2	−0.3	−0.1	−0.1	0.0	—	0.0

3.3. Average fission trajectory

Fig. 5a shows examples of the static fission trajectories obtained for three isotopes of Cm ($A = 238, 248, 258$). One can see that they differ rather much. The differences are the effect of differences in the shell structure of the isotopes. The solid line $\tilde{L}$(Cm) is an average static trajectory obtained from the trajectories calculated for 14 isotopes of Cm ($A = 234$–260). The trajectory $\tilde{L}$(Cm) is compared in Fig. 5b with the average trajectory $\tilde{L}_{DT}$(Cm), obtained for the same 14 isotopes of Cm but with only smooth (droplet) part of the potential energy, i.e. without the shell correction. It is seen that, despite of the averaging of the shell correction over the 14 isotopes, some shell effect remains and it is largest in the region of the first minimum (equilibrium deformation). Fig. 5c shows the trajectory $\tilde{L}$ averaged over 98 isotopes of seven elements ($Z = 92$–104). Using this trajectory, we construct a simple average trajectory $\bar{L}$, composed of three straight-line segments

$$\bar{\varepsilon}_6 = \begin{cases} 0.150 & \text{for} \quad 0.20 \leqslant \varepsilon \leqslant 0.30, \\ 0.150 - 1.125(\varepsilon - 0.30) & \text{for} \quad 0.30 \leqslant \varepsilon \leqslant 0.50, \\ -0.075 & \text{for} \quad 0.50 \leqslant \varepsilon \leqslant 1.00. \end{cases} \tag{9}$$

A smaller effect of the shell correction on the fission trajectory in the large (saddle-point) deformation region than in the region of small (equilibrium) deformations, observed in Fig. 5b, is connected with two facts. One is a smaller shell correction, itself, and the other is a larger stiffness of the smooth (droplet-model) part of the potential energy with respect

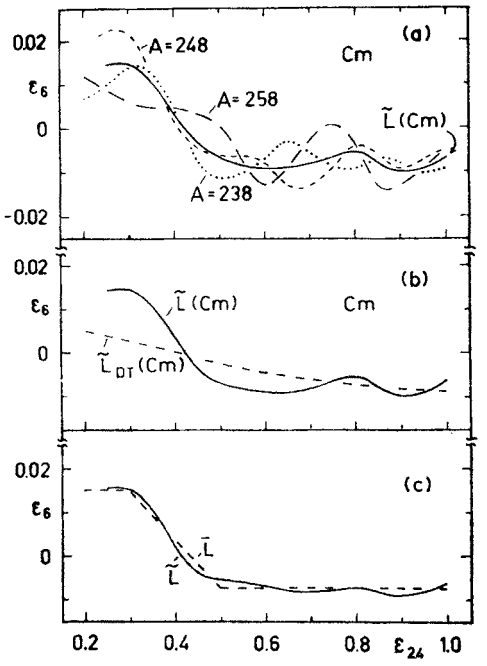

Fig. 5. Examples of the static fission trajectories calculated for three isotopes of Cm and an average trajectory, $\tilde{L}$(Cm), obtained from the trajectories for 14 isotopes of Cm (A = 234–260) (a). The average trajectory $\bar{L}$(Cm) as compared with that obtained in the droplet model $\tilde{L}_{DT}$(Cm) (b). A schematic average trajectory $\bar{L}$, derived from the average trajectory $\tilde{L}$, which is obtained from the trajectories calculated for 98 nuclides of the seven elements: Z = 92–104 (c)

to the ε_6-deformation in the saddle-point region than in the equilibrium region. The latter fact is illustrated in Fig. 6. The stiffness (second derivative) of the droplet-model potential energy V_{DT} with respect to ε_6 is by around 60% higher for ε = 0.80 than for ε = 0.25.

A map of the smooth (droplet-model) part of the potential energy, plotted as a function of the deformations ε_{24} and ε_6 is given in Fig. 7. It is seen that this energy is much flatter than the total energy given in Fig. 1.

3.4. Equilibrium deformations

It is interesting to study the equilibrium values of ε_6. For actinides, these quantities have not yet been calculated, except for unpublished calculations by Möller [8]. The latter were obtained with other parameters of the single-particle potential than used in the present paper. There were performed, a long time ago, some calculations of ε_6 for rare-earth nuclei [5]. They were, however, of rather preliminary nature as they did not use the normalization of the energy to the liquid drop.

Although only few, there exist now some experimental data for this high-multipolarity deformation of actinide nuclei, obtained from scattering of protons [9, 10] and alpha particles [11]. The data are for ^{232}Th and ^{234,236,238}U.

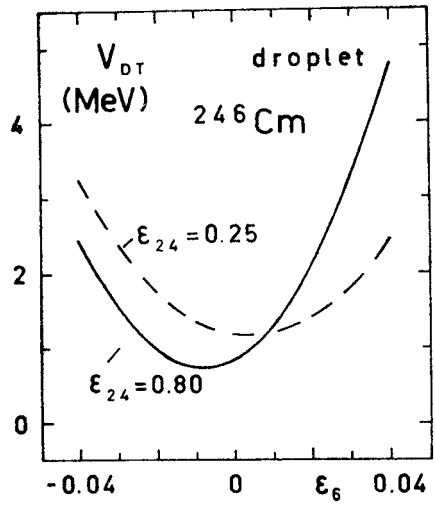

Fig. 6. Smooth (droplet-model) part of the potential energy V_{DT} plotted as a function of ε_6 for small ($\varepsilon_{24} = 0.25$) and large ($\varepsilon_{24} = 0.80$) quadrupole deformations

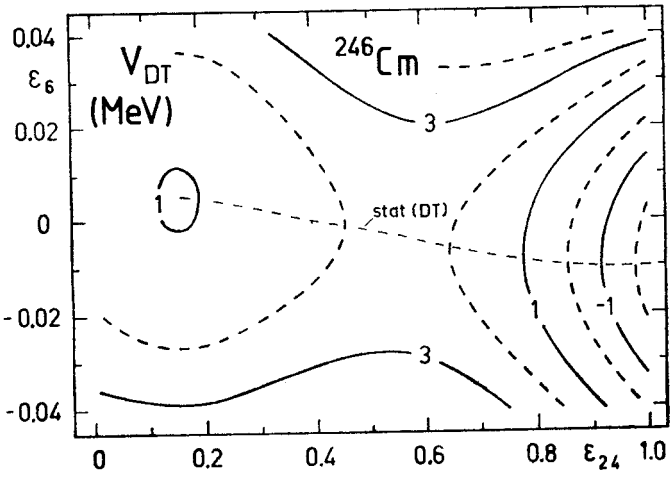

Fig. 7. Map of the droplet-model potential energy V_{DT} plotted as a function of ε_{24} and ε_6 for ^{246}Cm. No minimization of the energy with respect to ε_4 and ε_{35} is performed here. Static fission trajectory, stat (DT), obtained with this energy is also shown

Table III gives the calculated equilibrium values of ε, ε_4 and ε_6, the static electric moment Q_6^0, the total deformation energy E_{def} and the contribution ΔE_6 to this energy, due to the ε_6 degree of freedom. The static moment Q_6^0 is calculated at the equilibrium point $(\varepsilon^0, \varepsilon_4^0, \varepsilon_6^0)$ of a nucleus by the formula

$$Q_6^0 = 2 \int \varrho_p(r) r^6 P_6(\cos \vartheta) d\tau,$$

TABLE III

Equilibrium deformations ε^0, ε_4^0, ε_6^0 and static electric moment Q_6^0 for nuclei specified in the first two columns. The total deformation energy E_{def} and its part ΔE_6, due to the ε_6 deformation, are also given

Z	A	ε^0	ε_4^0	ε_6^0	Q_6^0	ΔE_6	E_{def}
—	—	—	—	—	b^3	MeV	MeV
92	240	0.218	−0.027	0.015	0.259	0.24	7.5
	242	0.221	−0.018	0.017	0.151	0.31	8.0
	240	0.218	−0.034	0.015	0.345	0.20	7.9
94	242	0.225	−0.025	0.017	0.248	0.32	8.6
	244	0.227	−0.017	0.019	0.140	0.37	9.1
	246	0.226	−0.008	0.020	0.027	0.40	9.2
	242	0.223	−0.030	0.015	0.334	0.25	8.7
	244	0.231	−0.021	0.019	0.206	0.42	9.6
96	246	0.232	−0.013	0.020	0.103	0.47	10.1
	248	0.232	−0.005	0.021	0.000	0.51	10.2
	250	0.229	0.003	0.020	−0.079	0.45	9.8
	242	0.218	−0.031	0.013	0.360	0.19	8.0
	244	0.230	−0.024	0.018	0.258	0.39	9.3
	246	0.235	−0.016	0.021	0.138	0.54	10.2
98	248	0.236	−0.008	0.022	0.033	0.60	10.8
	250	0.236	0.000	0.023	−0.073	0.63	10.9
	252	0.234	0.008	0.022	−0.152	0.56	10.6
	254	0.232	0.016	0.021	−0.227	0.48	10.1
	244	0.225	−0.024	0.016	0.271	0.29	8.3
	246	0.234	−0.017	0.020	0.165	0.47	9.6
	248	0.239	−0.009	0.023	0.041	0.64	10.6
100	250	0.240	−0.002	0.025	−0.070	0.71	11.2
	252	0.239	0.006	0.025	−0.166	0.73	11.4
	254	0.238	0.014	0.024	−0.244	0.66	11.2
	256	0.235	0.022	0.023	−0.322	0.57	10.7
	258	0.232	0.029	0.021	−0.370	0.48	10.1
	252	0.239	0.003	0.024	−0.119	0.66	11.0
	254	0.239	0.012	0.024	−0.225	0.69	11.3
102	256	0.237	0.020	0.023	−0.304	0.63	11.2
	258	0.234	0.027	0.022	−0.371	0.53	10.8
	260	0.231	0.035	0.020	−0.429	0.45	10.2

where the proton density distribution ϱ_p is assumed uniform, with sharp surface. Radius of a spherical nucleus, with the same volume as that of the deformed one, is taken as $R_0 = 1.2\,A^{1/3}$ fm.

The deformation energies are defined as

$$E_{def} = E(0, 0, 0) - E(\varepsilon^0, \varepsilon_4^0, \varepsilon_6^0), \tag{10}$$

$$\Delta E_6 = E(\varepsilon^0, \varepsilon_4^0, 0) - E(\varepsilon^0, \varepsilon_4^0, \varepsilon_6^0). \tag{11}$$

The results are presented only for nuclei for which the energy ΔE_6 is not too small. We, rather arbitrarily, put the condition $\Delta E_6 \gtrsim 0.2$ MeV.

Similarly as the static fission trajectory, the equilibrium deformations, corresponding to the point of minimal energy on this trajectory, is found in the two-dimensional analyses. The values ε^0 and ε_4^0 are found by minimization of the energy

$$V(\varepsilon, \varepsilon_4, 0, 0)+\Delta V_6$$

(cf. Eq. (5)) in the $(\varepsilon, \varepsilon_4)$-plane. It is worth mentioning that these values are only very little altered when the correction ΔV_6 is disregarded. The ε_6^0 value is found by minimization of the energy

$$V(\varepsilon, \bar{\varepsilon}_4, 0, \varepsilon_6)+\Delta V_4$$

in the $(\varepsilon_{24}, \varepsilon_6)$-plane.

One can see in Table III that the values of ε^0, obtained for the 31 nuclides specified in the table, fall into a very small interval, $\varepsilon^0 = 0.22$–0.24. The values of ε_4^0 are spread over

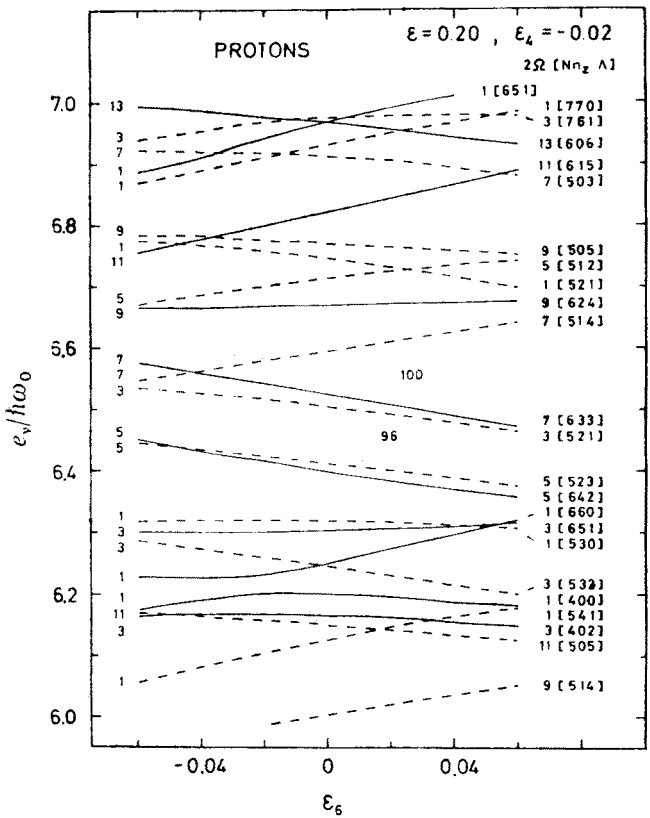

Fig. 8. Dependence of the proton single-particle levels on the deformation ε_6 for $\varepsilon = 0.2$, $\varepsilon_4 = -0.02$. The levels are labeled by $2\Omega[Nn_z \Lambda]$. The value of 2Ω is also repeated on the left-hand side of each level for easier identification. Position of the Fermi levels for $Z = 96$ and $Z = 100$ are indicated, for a pointer

a rather large region, $\varepsilon_4^0 = -0.034$–0.035, and the values of ε_6^0 again extend over a relatively small interval, $\varepsilon_6^0 = 0.013$–0.025. The total deformation energy is large, $E_{\text{def}} = 7.5$–-11.4 MeV, what means that the nuclei are well deformed. The contribution ΔV_6 to this energy is, however, small, not exceeding 0.73 MeV. The meaning of the latter may be found by comparing the values of ΔE_6 with the values of the zero-point energy corresponding to ε_6, treated as a separate degree of freedom, not coupled to other degrees. This energy may be estimated by considering it as half the vibrational energy $\hbar\omega_6$, which in the adiabatic approximation is

$$\hbar\omega_6 = \hbar\sqrt{C_{\varepsilon_6\varepsilon_6}/B_{\varepsilon_6\varepsilon_6}}, \tag{12}$$

where $C_{\varepsilon_6\varepsilon_6}$ is the stiffness of the potential energy with respect to ε_6. This way, one obtains for ^{246}Cm more than 4 MeV for $\hbar\omega_6$. Assuming that this estimate is about two times, or even slightly more, too high, similarly as it is for the quadrupole vibrations [12–14], one may roughly assume $\hbar\omega_6$ to be around 2 MeV and, consequently, the zero-point energy, $\frac{1}{2}\hbar\omega_6$, around 1 MeV.

Thus, the zero-point energy is large with respect to the deformation energy ΔE_6 given in Table III. This suggests that the deformation ε_6 of the nuclei given in the table has

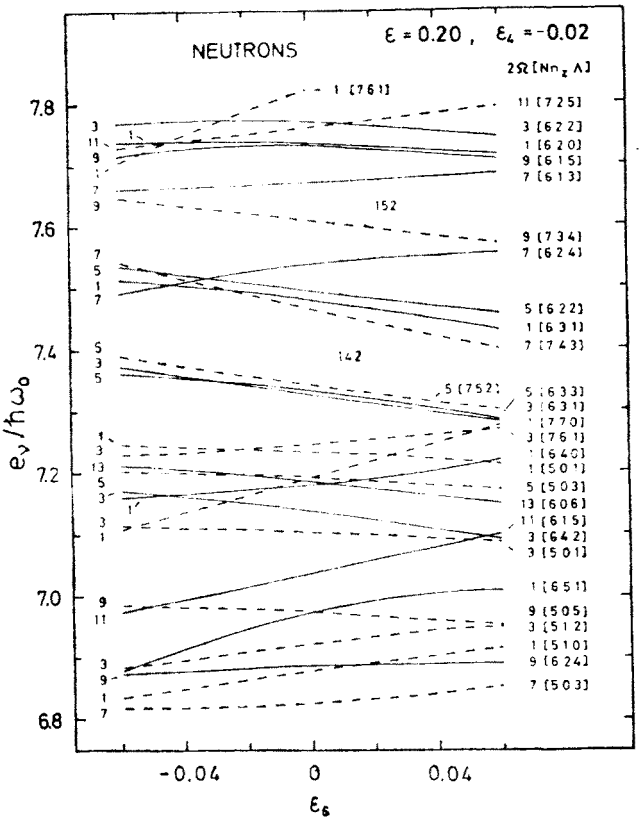

Fig. 9. Same as Fig. 8 but for neutrons

a dynamic rather than static character or, in other words, that the static values ε_6^0 given in the table are importantly changed by the dynamic corrections. This especially concerns the light isotopes of uranium: ^{234,236,238}U for which the experimental data for the deformation of multipolarity six exist [9–11]. The calculated values of ΔE_6 for these isotopes are 0.01, 0.06 and 0.12 MeV, respectively. Thus, the deformation ε_6 is expected to be of completely dynamic nature for them. This is the reason that we do not give the ε_6^0 values for these nuclides in Table III and that we do not compare these values with experiment. Such comparison needs the values calculated dynamically, i.e. with knowledge of the ground-state wave function as a function of deformations ε, ε_4 and ε_6.

It may be added that the values of ε^0 and ε_4^0 obtained and given, for completeness, in Table III in addition to ε_6^0 are rather close to those obtained by Möller [15].

3.5. Dependence of the single-particle levels on ε_6

Dependence of the single-particle energies e_ν on the deformation ε_6 is illustrated in Fig. 8 for protons and in Fig. 9 for neutrons. Values of the quadrupole and hexadecapole deformations, $\varepsilon = 0.2$, $\varepsilon_4 = -0.02$, are taken at the point which is close to the average equilibrium point for considered nuclei. The levels are labeled by (twice the) projection of spin on the symmetry axis, 2Ω, and the asymptotic quantum numbers $[Nn_z\Lambda]$. The parity is specified graphically: positive ($\pi = +$) parity by solid line and negative ($\pi = -$) parity by dashed line.

The dependence of e_ν on ε_6 is found more flat than the dependence on ε_4.

4. Conclusions

The following conclusions may be drawn from our study.

(1) The dynamic correction to the spontaneous-fission half-life $\Delta T_6^{\mathrm{dyn}}$ (due to an accounting for the deformation ε_6) is largest for heaviest nuclei and may change the lifetimes by up to about four orders. Most of it comes from the dependence of the potential energy on ε_6 (as described by ΔT_6^V). Considered as a function of the neutron number N, it has a maximum at $N \approx 152$–154.

(2) Diagonal components $B_{\varepsilon_6\varepsilon_6}$ of the microscopic mass tensor are about two times smaller, on the average, than the components $B_{\varepsilon_{24}\varepsilon_{24}}$.

(3) Small values of the mixed component $B_{\varepsilon_{24}\varepsilon_6}$, which fluctuate around zero with amplitude about 100 $\hbar^2$ MeV^{-1}, indicate that the ε_{24} and ε_6 degrees of freedom may be in good approximation considered as normal coordinates in all investigated region of deformations.

(4) Even for well deformed nuclei, with well established values of ε and ε_4, the deformation ε_6 is of a rather dynamic than static nature. Due to small values of the deformation energy corresponding to this degree of freedom, ΔE_6, large dynamical corrections to the static values ε_6^0 are expected.

The authors would like to thank Dr. A. Łukasiak for helpful discussions and his contribution during the initial stage of this research. Useful discussions with Drs. K. Pomorski and B. Zwięgliński are gratefully acknowledged.

REFERENCES

[1] A. Baran, K. Pomorski, S. E. Larsson, P. Möller, S. G. Nilsson, J. Randrup, A. Sobiczewski, Proc. 3rd Int. Conf. on nuclei far from stability, Cargèse 1976, CERN 76–13, Geneva 1976, p. 537.

[2] A. Baran, K. Pomorski, S. E. Larsson, P. Möller, S. G. Nilsson, J. Randrup, A. Łukasiak, A. Sobiczewski, *Physics and chemistry of fission* 1979, IAEA, Vienna 1980, vol. 1, p. 143.

[3] A. Baran, K. Pomorski, A. Łukasiak, A. Sobiczewski, *Nucl. Phys.* **A361**, 83 (1981).

[4] M. Brack, J. Damgaard, A. S. Jensen, H. C. Pauli, V. M. Strutinsky, C. Y. Wong, *Rev. Mod. Phys.* **44**, 320 (1972).

[5] S. G. Nilsson, C. F. Tsang, A. Sobiczewski, Z. Szymański, S. Wycech, C. Gustafson, I. L. Lamm, P. Möller, B. Nilsson, *Nucl. Phys.* **A131**, 1 (1969).

[6] W. D. Myers, W. J. Świątecki, *Ann. Phys.* (N.Y.) **84**, 186 (1974).

[7] W. D. Myers, *Droplet model of atomic nuclei* IFI/Plenum, New York 1977.

[8] P. Möller, private communication.

[9] J. M. Moss, Y. D. Terrien, R. M. Lombard, C. Brassard, J. M. Loiseaux, F. Resmini, *Phys. Rev. Lett.* **26**, 1488 (1971).

[10] R. M. Ronningen, R. C. Melin, J. A. Nolen, Jr., G. M. Crawley, *Phys. Rev. Lett.* **47**, 635 (1981).

[11] D. L. Hendrie, B. G. Harvey, J. R. Meriwether, J. Mahoney, J. C. Faivre, D. G. Kovar, *Phys. Rev. Lett.* **30**, 571 (1973).

[12] K. Pomorski, T. Kaniowska, A. Sobiczewski, S. G. Rohoziński, *Nucl. Phys.* **A283**, 394 (1977).

[13] S. G. Rohoziński, J. Dobaczewski, B. Nerlo-Pomorska, K. Pomorski, *Nucl. Phys.* **A292**, 66 (1977).

[14] A. Gyurkovich, A. Sobiczewski, S. G. Rohoziński, *Nucl. Phys.* **A383**, 77 (1982).

[15] P. Möller, *Nucl. Phys.* **A192**, 529 (1972).